Available online at www.sciencedirect.com
ScienceDirect
Ceramics International 35 (2009) 3005–3011
CERAMICS INTERNATIONAL
www.elsevier.com/locate/ceramint

Structure characterization and mechanical properties of CeO_2–ZrO_2 solid solution system

Yen-Pei Fu [a,*], Shao-Hua Hu [b], Biing-Lang Liu [c]

[a] Department of Materials Science and Engineering, National Dong Hwa University, Shou-Feng, Hualien 974, Taiwan
[b] Department of Environmental Resources Management, Dahan Institute of Technology, Sincheng, Hualien 971, Taiwan
[c] Department of Chemical Engineering, Wu Feng Institute of Technology, Ming Hsiung, Chiayi 621, Taiwan

Received 3 November 2008; received in revised form 5 March 2009; accepted 2 April 2009
Available online 24 April 2009

Abstract

The measured and calculated lattice parameters, microstructures, and mechanical properties (fracture toughness and microhardness) of CeO_2–ZrO_2 system ceramics are investigated, using CeO_2–ZrO_2 solid solution powder prepared by a microwave-induced combustion process. The CeO_2–ZrO_2 solid solution ceramics were sintered at 1500 °C for 6 h in air; the density of all specimens was greater than 94% of the theoretical density. For $Ce_{1-x}Zr_xO_2$ ($0.00 \leqq x \leqq 0.50$), the measured lattice parameter is in accordance with that of Kim's doped CeO_2 model. On the other hand, for $x \geqq 0.50$, the measured values fit Kim's doped ZrO_2 model. The fracture toughness and microhardness of CeO_2–ZrO_2 system ceramics with various compositions were investigated with Vickers indentation. The results showed that the crack mode of CeO_2–ZrO_2 solid solution was Palmqvist cracks under loads of 1 kg. Generally, the fracture toughness should increase with grain size at the submicron scale. However, larger grains may lead to spontaneous transformation, which should decrease the potential toughening at room temperature. This behavior was observed in the $Ce_{0.25}Zr_{0.75}O_2$ ceramic, which demonstrated a high fracture toughness that may be ascribed to two causes: (1) fine grain size and (2) transformation toughening.

Keywords: A. Powders: chemical preparation; C. Mechanical properties; D. CeO_2; D. ZrO_2; E. Fuel cells

1. Introduction

Nano powders have many excellent properties suitable for various applications such as ceramics, gas sensors, rechargeable batteries, and solid oxide fuel cells. In addition, they can significantly enhance sintering rates, decrease sintering temperatures, and improve optical, electric, and magnetic properties compared with micrometer-size powders [1,2]. Several synthesis routes have been developed to produce nanocrystalline CeO_2–ZrO_2 solid solution powders, such as the sol–gel method [3–5], thermal decomposition of cerium zirconyl oxalate under an argon flow [6], surfactant-assisted preparation [7], molten salt preparation [8], and combustion [9–11]. CeO_2-based powders have been synthesized successfully via combustion synthesis using different complexing agents/fuel, such as glycine [9,10] and carbohydrazide [12]. With combustion synthesis, a desired homogeneous high-purity powder can be produced in a short time and at a low cost.

In our current research, we attempted a new method of synthesis, termed the microwave-induced combustion process, to synthesize CeO_2–ZrO_2 solid solution powders. The advantages of our combustion method are (1) simple processing, because all the reactions take only a few minutes, in contrast to other methods that require tedious processing; (2) simple equipment, because this method does not require complicated equipment; and (3) cheap sources, because the chemicals used in this method are not expensive, unlike the special materials required for the sol–gel process. The microwave processing of materials is fundamentally different from conventional processing in terms of the heating mechanism. In a microwave oven, heat is generated within the sample itself by the interaction of microwaves with the material. In conventional heating, the heat is generated by heating elements, and is then transferred to the sample surfaces [13]. Microwave-induced combustion synthesis involves the dissolution of metal nitrates and urea in water, and then the

* Corresponding author. Tel.: +886 3 863 4209; fax: +886 3 863 4200.
E-mail address: d887503@alumni.nthu.edu.tw (Y.-P. Fu).

0272-8842/$36.00
doi:10.1016/j.ceramint.2009.04.001

heating of the solution in a microwave oven. The urea and metal nitrates decompose and give off flammable gases. After the solution reaches the point of spontaneous combustion, it begins to burn and becomes a solid, which burns at a high temperature. Combustion is not complete until all the flammable substances are consumed, and the resulting material is a loose, highly friable substance exhibiting voids and pores formed by the escaping gases during the combustion reaction [14].

There have been many investigations of the oxygen storage properties [15], thermal stability [16], redox properties [4], and catalysts conversion [17] of CeO_2–ZrO_2 solid solution powders, which have focused on correlations between catalysts properties and composition. There seem to be few studies, however, on the mechanical properties of CeO_2–ZrO_2 system ceramics. Therefore, in this article, we report the lattice parameters, microstructures, fracture toughness, and microhardness of $Ce_{1-x}Zr_xO_2$ ceramics ($0.00 \leqq x \leqq 0.75$).

2. Experimental procedures

2.1. Sample synthesis

The synthesis process involved the combustion of redox mixtures, in which metal nitrate acted as the oxidizing reactant and urea as the reducing reactant. The initial composition of the solution contained cerium nitrate, zirconyl nitrate dihydrate, and urea and was based on the total oxidizing and reducing valences of the oxidizer and the fuel, relying on concepts from the propellant chemistry [18,19]. The detailed experimental procedure to synthesize CeO_2–ZrO_2 solid solution powder by microwave-induced combustion is described elsewhere [20]. Stoichiometric amounts of cerium nitrate hexahydrate ($Ce(NO_3)_3{\cdot}6H_2O$), zirconyl nitrate dihydrate ($ZrO(NO_3)_2{\cdot}2H_2O$), and urea ($CO(NH_2)_2$) were dissolved in a minimal quantity of water and placed in a crucible. A 15 ml of solution containing nitrates and urea was added to a crucible. The crucible was then introduced into a microwave oven (CEM, MDS 81D, 650 W). Initially, the solution boiled and underwent dehydration followed by decomposition accompanied by the evolution of a large amount of gases (N_2, NH_3, and HNCO). After the solution reached the point of spontaneous combustion, it began to burn, released heat, vaporized all the solution instantly and became a solid burning at a temperature of over 1000 °C. The entire combustion process produced CeO_2–ZrO_2 solid solution powders in a microwave oven in only 15 min. These powder samples were annealed at 600 °C for 2 h, and then pelletized and sintered at 1500 °C for 6 h.

2.2. Characterization

A computer-interface X-ray powder diffractometer (XRD) with Cu K_α radiation (Rigaku D/Max-II, Tokyo, Japan) was used to identify the crystalline phase and calculate crystallite size. The crystalline size, D_{XRD} was calculated according to the Scherer equation: $D_{XRD} = 0.9\lambda/B\cos\theta$, where λ is the wavelength of the radiation, and θ is the diffraction angle. B is the corrected half-width of the diffraction peak, given by $B^2 = B_m^2 - B_s^2$, where B_m is the measured half-width of the diffraction peak, and B_s is the half-width of standard CeO_2 with a crystal size greater than 100 nm. The reflection from the (1 1 1) plane, occurring at 28.6° 2Θ, was used to calculate the crystallite size. The BET surface area measurements were made based on nitrogen adsorption employing a Micromeritics ASAP 2000 instrument and calculated using the five-point Brunauer–Emmit–Teller (BET) theory. Mean particle size (D_{BET}) was calculated from the BET data according to $D_{BET} = 6/(\rho_{th}S_{BET})$, where S_{BET} is the measured surface area, and ρ_{th} is the theoretical density of the compound.

Vickers hardness was measured using a microhardness tester (Akashi MVK-H110, Tokyo, Japan) with a load of 1000 g held for 10 s. At least 10 indentations were used to obtain the mean and standard deviation values of hardness and fracture toughness. All specimens were polished with a series of emery papers of 800, 1000, 1200, and 1500 grit. Contamination on the surface was ultrasonically cleaned with ethanol. The Vickers indenter hardness was determined by the average value of both diagonals with a Vickers indenter apex of 136° and calculated with the following equation: $H_V = 1.8544 \times (P/d^2)$ where P is the load, and d is the mean value of both diagonals. The morphological features of the CeO_2–ZrO_2 system ceramics were observed using a scanning electron microscope (SEM; Hitachi S-3500H, Tokyo, Japan).

3. Results and discussion

The X-ray diffraction patterns of the CeO_2–ZrO_2 solid solution powders prepared via the microwave-induced combustion process were identified with a diffractometer. Fig. 1 shows that the $Ce_{1-x}Zr_xO_2$ ($0.00 \leqq x \leqq 0.75$) powders contain only the cubic fluorite structure with space group *Fm3m* (JCPDS powder diffraction File No. 34-0394). The formation of a single phase is due to the high temperature generated in situ during combustion and to the rapid cooling rate. Such a high temperature could provide energy to produce zirconium-doped cerium oxide powder from the solution during combustion. The

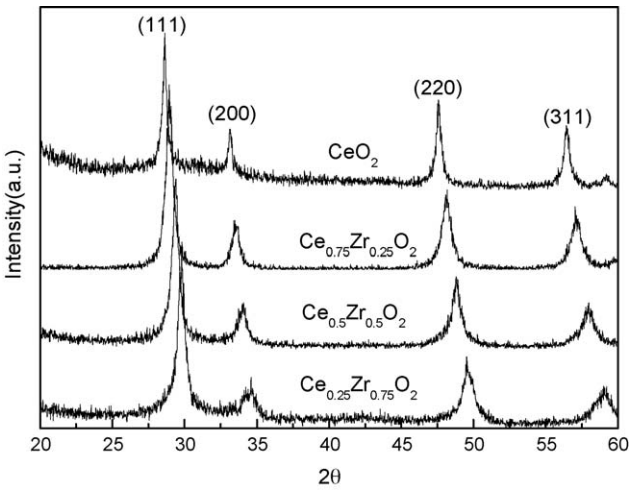

Fig. 1. XRD patterns of $Ce_{1-x}Zr_xO_2$ ($0.00 \leqq x \leqq 0.75$) powders synthesized by microwave-induced combustion.

XRD peaks are quite broad and indicate the fine particle size of the product. The primary crystalline size determined from the Scherer equation is in the range of 8–16 nm. When using the Scherer equation, we assume that the particle size effects are only peak broadening; however, if the particles are non-uniform, the particle size will be underestimated. The mean particle size (D_{BET}) can be obtained from the BET data. When calculating the mean particle size, we assume that the particles are spherical. The results revealed that the specific surface area is a distribution in the range of 42–48 m^2/g, and the mean particle size is in the range of 17–20 nm. The specific surface areas, mean particle sizes and crystallite sizes of CeO_2–ZrO_2 solid solution powders are listed in Table 1. It is well known that $\psi = D_{BET}/D_{XRD}$ which is a factor that reflects the extent of agglomeration of the primary crystallites. D_{BET} values are always larger than D_{XRD} values, which is a result of the small agglomerates that occur in CeO_2–ZrO_2 solid solution powders, leading to N_2 gas being unable to completely penetrate agglomerates during BET analysis. Moreover, XRD can detect the subgrains within particles. With increasing Zr substitution, the ψ value increased gradually from 1.18 to 2.10. We conclude that the extent of agglomeration increases with Zr substitution for CeO_2–ZrO_2 solid solution powders. Fig. 2 shows the XRD patterns of CeO_2–ZrO_2 system ceramics sintered at 1500 °C with the fluorite structure for Zr substitution in the range of $x = 0.00$–0.50. No secondary phases are found in this Zr substitution range. However, when the substitution of Zr reached 0.75, both the tetragonal structure of ZrO_2 and the cubic structure of CeO_2 appeared in the $Ce_{0.25}Zr_{0.75}O_2$ ceramics. These results demonstrate that the structure of $Ce_{1-x}Zr_xO_2$ ceramics depends on x. For $x \leqq 0.5$ the phase is only CeO_2 (cubic solid solution), while if $x = 0.75$ the major phase is CeO_2 (cubic solid solution) with a minor ZrO_2 (tetragonal solid solution) phase. The phase equilibrium of the CeO_2–ZrO_2 system is shown in Fig. 3 [21]. It is clear that the CeO_2–ZrO_2 solid solution system contains two phases (tetragonal + cubic) within the solubility of 82 mol% CeO_2 in ZrO_2 at room temperature. Therefore, the results of X-ray diffraction for the CeO_2–ZrO_2 system are consistent with the phase diagram.

Shannon and Prewitt [22] reported that the ionic radii of Ce^{4+} and Zr^{4+} for a coordination number of 6 are 0.080 and 0.072 nm, respectively, whereas for a coordination numbers of 8 the values are 0.097 and 0.084 nm, respectively. The coordination number is equivalent to 8 for the CeO_2–ZrO_2 solid solution. Calculation of the cell parameters was carried out using the four main reflections typical of a fluorite structure material with a fcc cell, corresponding to the (1 1 1), (2 0 0), (2 2 0), and (3 1 1) planes. The different radii of Ce^{4+} (0.097 nm) and Zr^{4+} (0.084 nm) lead the lattice constant to decrease with increasing Zr substitution for CeO_2–ZrO_2 solid solution ceramics. Zr substitution for Ce in the CeO_2–ZrO_2 system induces a uniform strain in the lattice as the material is elastically deformed. This effect causes the lattice plane spacing to change and the diffraction peaks to shift to new 2θ position. The structural characterization and lattice parameters are summarized in Table 2. It was found that with increasing Zr substitution for Ce, the lattice parameter decreases for the cubic phase. When $x = 0.75$, the zirconia–ceria system contains two types of phases. The lattice parameters of the two structures are $a = 5.174$ Å for the cubic structure and $a = 3.145$ Å, $b = 3.145$ Å, $c = 9.118$ Å for the tetragonal structure. Kim [23]

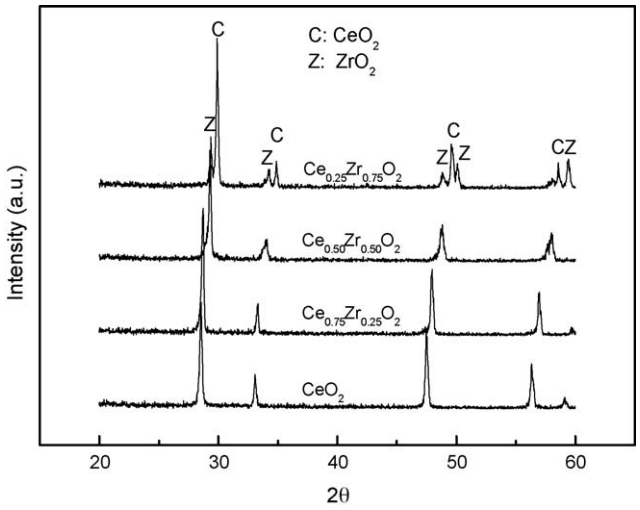

Fig. 2. XRD patterns of $Ce_{1-x}Zr_xO_2$ ($0.00 \leqq x \leqq 0.75$) ceramics sintered at 1500 °C for 6 h.

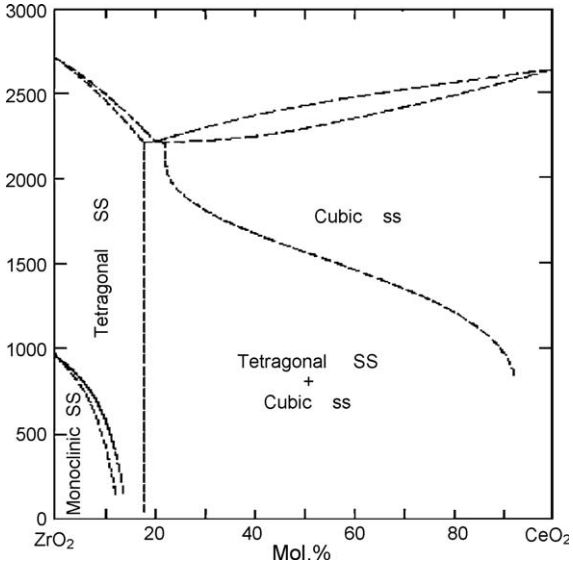

Fig. 3. Phase equilibrium of the CeO_2–ZrO_2 system [21].

Table 1
Specific surface area, particle size, and crystallite size of CeO_2–ZrO_2 solid solution powders synthesized by microwave-induced combustion process.

Composition	Specific surface area (m^2/g)	Particle size[a] (nm)	Crystallite size[b] (nm)	ψ[c]
CeO_2	43.47	19.14	16.18	1.18
$Ce_{0.75}Zr_{0.25}O_2$	45.33	18.35	9.73	1.88
$Ce_{0.50}Zr_{0.50}O_2$	42.18	19.73	10.25	1.92
$Ce_{0.25}Zr_{0.75}O_2$	48.62	17.12	8.14	2.10

[a] Particle size measured from specific surface area.
[b] Crystallite size measured from XRD line broadening.
[c] ψ = Particle size/crystallite size.

Table 2
The structure, lattice parameters and theory density for CeO_2–ZrO_2 system ceramics.

Composition	Structure	Lattice parameters (Å)	Theory density (%)
CeO_2	Cubic	$a = 0.5411$	94.7
$Ce_{0.75}Zr_{0.25}O_2$	Cubic	$a = 0.5367$	95.6
$Ce_{0.50}Zr_{0.50}O_2$	Cubic	$a = 0.5271$	96.3
$Ce_{0.25}Zr_{0.75}O_2$	Cubic	$a = 0.5174$	94.2
	Tetragonal	$a = 0.3145$, $b = 0.3145$, $c = 0.9118$	

proposed an empirical equation for lattice parameter changes of fluorite oxide solid solutions described as follows:

(A) The empirical equation for the lattice parameter (a) of doped ceria (which is called, according to Kim's model doped CeO_2) is given by

$$(a) = 0.5413 + \sum_k (0.0220\Delta r_k + 0.00015\Delta z_k)m_k. \quad (1)$$

(B) The empirical equation for the lattice parameter (a) of doped zirconia (which is called, according to Kim's model doped ZrO_2) is given by

$$(a) = 0.5120 + \sum_k (0.0212\Delta r_k + 0.00023\Delta z_k)m_k. \quad (2)$$

where Δr_k is the difference in ionic radius ($r_k - r_h$) of the kth dopant (r_k) and the host cation (r_h) in eightfold coordination, Δz_k is the valency difference ($z_k - z_h$), and m_k is the mole percent of the kth dopant in the form of MO_x. In this study, the radius of Zr^{4+} is 0.084 nm, and that of Ce^{4+} is 0.097 nm. Fig. 4 shows the plot of the calculated and measured lattice parameters of CeO_2–ZrO_2 solid solutions. For $Ce_{1-x}Zr_xO_2$ ($0.00 \leqq x \leqq 0.50$), the experimental results are in accordance with the lattice parameter of Kim's doped CeO_2 model. On the other hand, for $x \geqq 0.50$, the measured values fit in with Kim's doped ZrO_2 model. We also found that Kim's model is accurate

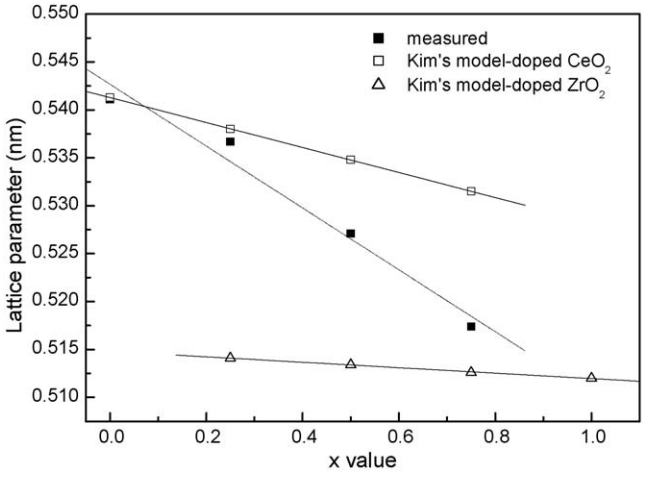

Fig. 4. Calculated and measured lattice parameter of CeO_2–ZrO_2 solid solution.

Table 3
Microhardness, and indentation length for CeO_2–ZrO_2 system ceramics.

Ceramic	Load P (kg)	Indentation length		Microhardness H_V (GPa)
		D_1 (μm)	D_2 (μm)	
CeO_2	1	60.6 ± 3.9	60.2 ± 3.6	4.99 ± 0.57
$Ce_{0.75}Zr_{0.25}O_2$	1	40.5 ± 1.5	43.0 ± 1.5	10.60 ± 0.40
$Ce_{0.50}Zr_{0.50}O_2$	1	40.2 ± 2.3	40.8 ± 1.1	11.03 ± 0.85
$Ce_{0.25}Zr_{0.75}O_2$	1	60.0 ± 4.4	58.4 ± 4.1	5.23 ± 0.78

for a small amount of dopant, but a heavy amount of dopant does not match the fluorite oxide solid solution lattice parameters very well.

The length of the diagonal line of indentation is denoted as D. A crack length of $2C$ is measured from the two ends of the crack. The Vickers hardness, indentation length, and crack length of CeO_2–ZrO_2 system ceramics are summarized in Table 3. In this study, microhardness was measured by applying a load of 1 kg using a diamond Vickers microhardness indenter. The fracture toughness vs. crack size was first examined based on the following equation [24]:

$$K_{IC} = 0.016\left(\frac{E}{H_V}\right)^{1/2}\left(\frac{P}{C^{3/2}}\right) \quad (3)$$

where K_{IC} is the fracture toughness, E is the Young's modulus, H_V is the Vickers hardness, P is the load and C is the half-crack size. There are many indentation equations to calculate K_{IC} as presented by Ponton and Rawling [25]. There are specific conditions and limitations for each formula; so far, no universal formula is available to evaluate K_{IC} for all ceramic materials [26]. In a later manuscript, we examined the crack system and found that Palmqvist cracks were observed under indentation loads of 1 kg for the CeO_2–ZrO_2 solid solution system. Although Eq. (3) is valid for a Penny-shape crack system, another equation should be used for a Palmqvist crack system. The fracture toughness for Palmqvist cracks in brittle materials can be obtained from the expression given by Niihara et al. [27] on the basis of the following equation

$$\left(\frac{K_{IC}\phi}{Ha^{1/2}}\right)\left(\frac{H}{E\phi}\right)^{2/5} = 0.035\left(\frac{c}{a}\right)^{-1/2} \quad (4)$$

where K_{IC} is the fracture toughness, H is the hardness, E is the Young's modulus, $2a = d$ is the diagonal of the indentation, c is the crack length and ϕ is the constraint factor $\fallingdotseq 3$. From this relation an expression for the fracture toughness can be obtained.

$$K_{IC} = 9.052 \times 10^{-3} H^{3/5} E^{2/5} d c^{-1/2} \quad (5)$$

However, for convenience and by comparing the result with others in the literature, Eq. (3) was applied for dealing with the indentation data of doped ceria-based ceramics. Fig. 5 depicts the fracture toughness and microhardness for $Ce_{1-x}Zr_xO_2$ ($0.00 \leqq x \leqq 0.75$) ceramics. The fracture toughness initially decreased with increasing ZrO_2 substitution in the range of $0.00 \leqq x \leqq 0.50$, whereas the microhardness increased. At $x = 0.75$, the ZrO_2 phase appeared in the CeO_2–ZrO_2 solid

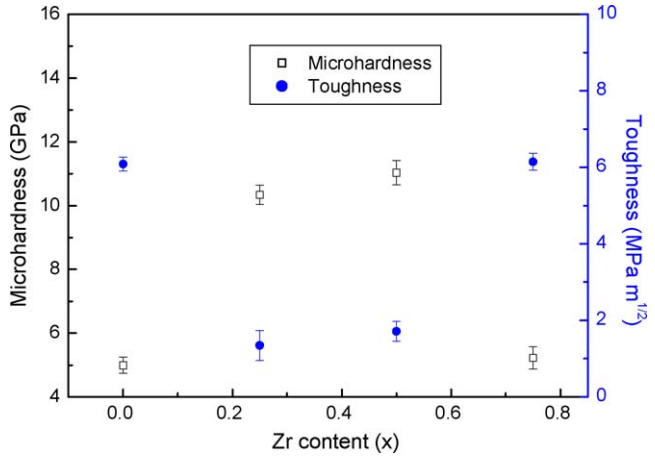

Fig. 5. Fracture toughness and microhardness for $Ce_{1-x}Zr_xO_2$ ($0.00 \leqq x \leqq 0.75$) ceramics.

solution. This is due to transformation toughening that occurs in $Ce_{0.25}Zr_{0.75}O_2$ ceramic. In general, zirconia is a polymorphous material. It exhibits three well-defined phases from low to high temperature: a monoclinic phase, a tetragonal phase, and a cubic phase. The low-temperature phase is monoclinic, stable up to 1170 °C at which temperature it changes reversibly to the tetragonal phase. The tetragonal-to-monoclinic ($t \rightarrow m$) transformation is associated with a large volume change and undergoes extensive shear, which is the basis for the transformation toughness of zirconia containing ceramics [28].

A Vickers indenter produces two types of crack systems, namely, a median crack system and a Palmqvist crack system. In general, the high toughness materials have a Palmqvist crack system, while low toughness materials exhibit a median crack system. Practically, most materials will exhibit both crack systems depending on the indenter load. A simple way to distinguish between these crack systems is to polish away the surface layer. The median crack system will always remain connected to the corner of the indent, whereas the Palmqvist crack system will become detached from the corner of the indent [29,30]. Fig. 6 shows the surface crack for a $Ce_{0.50}Zr_{0.50}O_2$ specimen, before and after being polished, and the Palmqvist crack can be observed under indentation loads of 1 kg. At low loads, Palmqvist cracks are favored, while

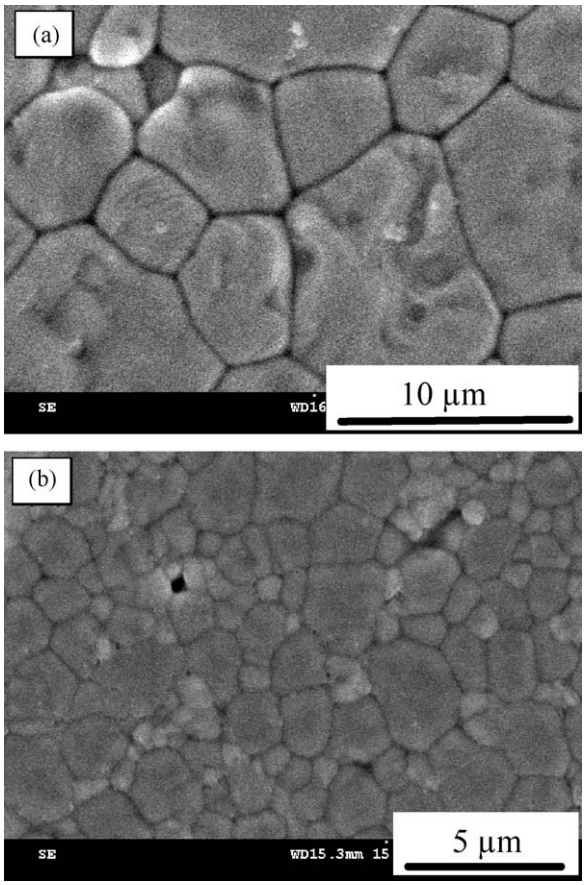

Fig. 7. SEM images for samples (a) $Ce_{0.75}Zr_{0.25}O_2$ and (b) $Ce_{0.25}Zr_{0.75}O_2$ sintered at 1500 °C for 6 h.

at high loads, fully developed median cracks result [28]. For example, Matsumoto [31] studied ceria-stabilized tetragonal zirconia polycrystal (Ce-TZP) materials, in which the Palmqvist crack system appears at low loads (<500 N), while the medium crack occurs at high loads (>600 N). Glandus et al. [30] proposed that an yttria-stabilized tetragonal zirconia polycrystal (Y-TZP) shows the Palmqvist cracks under indentation loads <500 N [32]. Similar behavior is observed in other CeO_2–ZrO_2 system ceramics. In this study, the occurrence of Palmqvist cracks is ascribed to the low indentation loads of 1 kg (9.8 N).

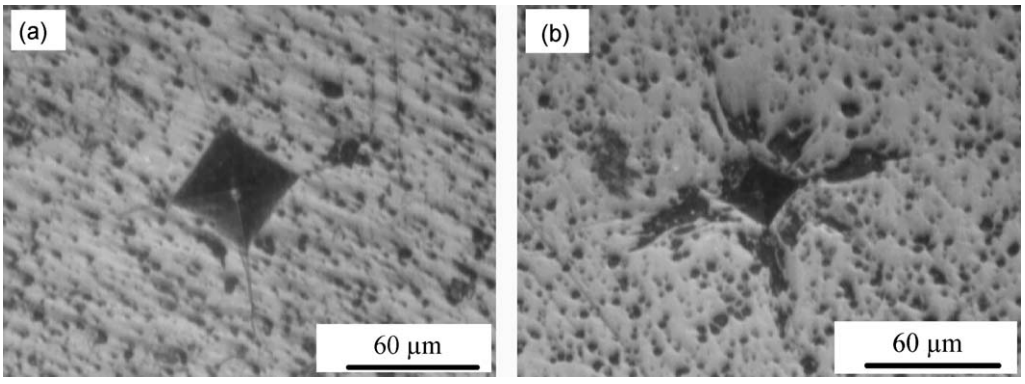

Fig. 6. The optical microscopy micrograph of indent under a load of 1 kg for $Ce_{0.50}Zr_{0.50}O_2$ ceramic (a) before and (b) after polishing.

SEM micrographs of the thermally etched $Ce_{0.75}Zr_{0.25}O_2$ and $Ce_{0.25}Zr_{0.75}O_2$ ceramics sintered at 1500 °C for 6 h are presented in Fig. 7. The main microstructural difference is that $Ce_{0.25}Zr_{0.75}O_2$ has significantly smaller grain size than $Ce_{0.75}Zr_{0.25}O_2$. In the Zr-rich $Ce_{1-x}Zr_xO_2$ solid solution, the appearance of the tetragonal phase of ZrO_2 may enhance grain-size refinement. In Fig. 7(a), the microstructure of $Ce_{0.75}Zr_{0.25}O_2$ ceramics reveals that high densification was achieved. There was little or no intergranular porosity found in any specimens, and the grain size was distributed in the range of 3–8 μm. In Fig. 7(b), the grain size is in the range of 1–4 μm, which is associated with the appearance of tetragonal ZrO_2. Fine grains can significantly increase fracture toughness. In general, the fracture toughness should increase with grain size at the submicron scale [33]. However, larger grains may lead to spontaneous transformation, which decreases the potential toughening at room temperature. This behavior was observed in a study of the CeO_2–ZrO_2 solid solution system [34]. According to XRD, toughness, and SEM results, we conclude that the high fracture toughness of the $Ce_{0.25}Zr_{0.75}O_2$ ceramic may be ascribed to two reasons: (1) fine grain size and (2) the occurrence of transformation toughening.

4. Conclusions

The lattice parameters, microstructures, density, and mechanical properties (fracture toughness, and microhardness) of the CeO_2–ZrO_2 system ceramics were investigated for CeO_2–ZrO_2 solid solution powders prepared via a microwave-induced combustion process using cerium nitrate hexahydrate, zirconyl nitrate dihydrate, and urea as the starting materials. All specimens of the CeO_2–ZrO_2 system had densities greater than 94% of the theoretical when sintered at 1500 °C for 6 h, which indicates that nanosize CeO_2–ZrO_2 solid solution powders prepared by the microwave-induced combustion process have high sinterability. For $Ce_{1-x}Zr_xO_2$ ($0.00 \leqq x \leqq 0.50$), the experimental results agree with the lattice parameter of Kim's doped CeO_2 model. On the other hand, for $x \geqq 0.50$, the measured values fit the Kim's doped ZrO_2 model. On the basis of optical microscopy observations, the dependence of crack length on indentation load of CeO_2–ZrO_2 system ceramics corresponds to Palmqvist cracks under loads of 1 kg. In general, the fracture toughness should increase with grain size at the submicron scale. However, larger grains may lead to spontaneous transformation, which decrease the potential toughening at room temperature. This behavior is observed in $Ce_{0.25}Zr_{0.75}O_2$ ceramic revealing high fracture toughness that may be attributed to two factors: (1) fine grain size and (2) transformation toughening.

Acknowledgement

The authors would like to thank the National Science Council of the Republic of China for financially supporting this research under Contract No. NSC 95-2221-E-259-023.

References

[1] H. Hahn, Sintering characteristics of nanocrystalline TiO_2, J. Mater. Res. 5 (1990) 609–614.
[2] Y.C. Zhou, M.N. Rahaman, Hydrothermal synthesis and sintering of ultrafine CeO_2 powders, J. Mater. Res. 8 (1993) 1680–1686.
[3] S. Rossignol, Y. Madier, D. Duprez, Preparation of zirconia–ceria materials by soft chemistry, Catal. Today 50 (1999) 261–270.
[4] M.F. Luo, G.L. Lu, X.M. Zheng, Redox properties of $Ce_xZr_{1-x}O_2$ mixed oxides prepared by the sol–gel method, J. Mater. Sci. Lett. 17 (1998) 1553–1557.
[5] M. Alifanti, B. Baps, N. Blangenois, J. Naud, P. Grang, B. Delmon, Characterization of CeO_2–ZrO_2 mixed oxides—comparison of the citrate and sol–gel preparation methods, Chem. Mater. 15 (2003) 395–403.
[6] T. Masui, T. Ozaki, K. Machida, G. Adachi, Effects of surface modification by chemical filing on the redox behavior of a ceria–zirconia mixed oxide, J. Alloys Compd. 292 (1999) 8–10.
[7] D. Terribile, A. Trovarelli, J. Lorca, C. de Leitenburg, G. Dolcetti, The preparation of high surface area CeO_2–ZrO_2 mixed oxides by a surfactant-assisted approach, Catal. Today 43 (1998) 79–88.
[8] P. Afanasiev, Ce–Zr mixed oxides prepared in molten nitrates, J. Alloys Compd. 340 (2002) 74–78.
[9] R.D. Purohit, B.P. Sharma, K.T. Pillai, A.K. Tyagi, Ultrafine ceria powder via glycine–nitrate combustion, Mater. Res. Bull. 36 (2001) 2711–2721.
[10] R. Peng, C. Xia, Q. Fu, G. Meng, D. Peng, Sintering and electrical properties of $(CeO_2)_{0.8}(Sm_2O_3)_{0.1}$ powders prepared by glycine–nitrate process, Mater. Lett. 56 (2002) 1043–1047.
[11] T. Mokkelbost, I. Kaus, T. Grande, M.-A. Einarsrud, Combustion synthesis and characterization of nanocrystalline CeO_2-based powders, Chem. Mater. 16 (2004) 5489–5494.
[12] J.J. Kingsley, K. Suresh, K.C. Patil, Combustion synthesis of fine-particle metal aluminates, J. Mater. Sci. Lett. 29 (1990) 1305–1312.
[13] D.E. Clark, W.H. Sutton, Microwave processing of materials, Ann. Rev. Mater. Sci. 26 (1996) 299–331.
[14] O.A. Lopez, J. McKittrick, L.E. Shea, Fluorescence properties of polycrystalline Tm^{+++}-activated $Y_3Al_5O_{12}$ and Tm^{+++}-Li^+ co-activated $Y_3Al_5O_{12}$ in the visible and near IR ranges, J. Lumin. 71 (1997) 1–11.
[15] C.E. Hori, H. Permana, K.Y.S. Ng, A. Brenner, K. More, K.M. Rahmoeller, D. Belton, Thermal stability of oxygen storage properties in a mixed CeO_2–ZrO_2 system, Appl. Catal. B: Environ. 16 (1998) 105–117.
[16] G. Colon, F. Valdivieso, M. Pijolat, R.T. Baker, J.J. Calvino, S. Bernal, Texture and phase stability of $Ce_xZr_{1-x}O_2$ mixed oxides under high temperature oxidizing conditions, Catal. Today 50 (1999) 271–284.
[17] M. Ozawa, M. Kimura, A. Isogai, The application of Ce–Zr oxide solid solution to oxygen storage promoters in automotive catalysts, J. Alloys Compd. 193 (1993) 73–75.
[18] R. Gopi Chandran, K.C. Patil, G.T. Chandrappa, Combustion synthesis, characterization, sintering and microstrucutre of mullite–cordierite composites, J. Mater. Sci. Lett. 14 (1995) 548–551.
[19] H.K. Park, Y.S. Han, D.K. Kim, C.H. Kim, Synthesis of $LaCrO_3$ powders by microwave induced combustion of metal nitrate–urea mixture solution, J. Mater. Sci. Lett. 17 (1998) 785–787.
[20] Y.P. Fu, C.H. Lin, Preparation of $Ce_xZr_{1-x}O_2$ powders by microwave-induced combustion process, J. Alloys Compd. 354 (2003) 232–235.
[21] P. Duwez, F. Dell, Phase relationships in the system zirconia–ceria, J. Am. Ceram. Soc. 33 (1950) 274–283.
[22] R.D. Shannon, C.T. Prewitt, Effective ionic radii in oxides and fluorides, Acta Cryst. B 25 (1969) 925–946.
[23] D.J. Kim, Lattice parameter, ionic conductivities, and solubility limits in fluorite-structure MO_2 oxide ($M = Hf^{4+}$, Zr^{4+}, Ce^{4+}, Th^{4+}, U^{4+}) solid solutions, J. Am. Ceram. Soc. 72 (1989) 1415–1421.
[24] G.R. Anstis, P. Chantikul, B.R. Lawn, D.B. Marshall, A critical evaluation of indentation techniques for measuring fracture toughness. I. Direct crack measurements, J. Am. Ceram. Soc. 64 (1981) 533–538.
[25] B.C. Ponton, R.D. Rawling, Vickers indentation fracture toughness test. Part 1. Review of literature and formulation of standard indentation toughness equations, Mater. Sci. Tech. 5 (1989) 865–872.

[26] J. Ma, T.S. Zhang, L.B. Kong, P. Hing, Y.J. Leng, S.H. Chan, Preparation and characterization of dense $Ce_{0.8}Y_{0.15}O_{2-\delta}$ ceramics, J. Eur. Ceram. Soc. 24 (2004) 2641–2648.
[27] K. Niihara, R. Morena, D.P.H. Hasselman, Evaluation of K_{IC} of brittle solids by the indentation method with low crack-to-indent ratios, J. Mater. Sci. Lett. 1 (1982) 13–16.
[28] M.W. Barsoum, Fundamentals of Ceramics, McGraw-Hill Companies, New York, 1997.
[29] R.L.K. Matsumoto, Elastic modulus–porosity relation in polycrystalline rare-earth oxides, J. Am. Ceram. Soc. 70 (1987) C362–C366.
[30] J.C. Glandus, T. Rouxel, Q. Tai, Study of the Y-TZP toughness by an indentation method, Ceram. Int. 17 (1991) 129–135.
[31] R.L.K. Matsumoto, Evaluation of fracture toughness determination methods as applied to ceria-stabilized tetragonal zirconia polycrystal, J. Am. Ceram. Soc. 70 (1987) C-366–C-368.
[32] J.D. Lin, J.G. Duh, Fracture toughness and hardness of ceria- and yttria-doped tetragonal zirconia ceramics, Mater. Chem. Phys. 78 (2002) 253–261.
[33] A. Bravo-Leon, Y. Morikawa, M. Kawahara, M.J. Mayo, Fracture toughness of nanocrystalline tetragonal zirconia with low yttria content, Acta Mater. 50 (2002) 4555–4562.
[34] R.H.J. Hanninh, Transformation toughening in zirconia-containing ceramics, J. Am. Ceram. Soc. 83 (2000) 461–487.